Engineering 55 (2025) 182–190

Contents lists available at ScienceDirect

Engineering

journal homepage: www.elsevier.com/locate/eng

Research
Nuclear Power—Article

Performance of the First 80 kA HTS CICC for High-Field Application in Future Fusion Reactors

Huan Jin [a], Guanyu Xiao [a], Chao Zhou [a,b,*], Chuanyi Zhao [a], Shijie Shi [a], Haihong Liu [a], Fang Liu [a], Huajun Liu [a], Yu Wu [a], Zuojiafeng Wu [c], Hugues Bajas [d], Jack Greenwood [d], Mattia Ortino [d], Kamil Sedlak [d], Valentina Corato [e], Richard Kamendje [f,g], Alexandre Torre [h], Arend Nijhuis [i], Giulio Anniballi [i], Arnaud Devred [j], Jinggang Qin [a,*], Yuntao Song [a], Jiangang Li [a]

[a] Institute of Plasma Physics, Chinese Academy of Sciences, Hefei 230031, China
[b] Institute of Energy, Hefei Comprehensive National Science Center, Hefei 230001, China
[c] Yichun Longteng Mechanical and Electrical Co., Ltd., Yichun 336000, China
[d] Swiss Plasma Center, École Polytechnique Fédérale de Lausanne, Villigen 5232, Switzerland
[e] ENEA Frascati Research Center, Frascati 00044, Italy
[f] EUROfusion, Garching 85748, Germany
[g] Institut für Theoretische Physik-Computational Physics, Graz 8010, Austria
[h] Commissariat à l'Energie Atomique et aux Energies Alternatives, Gif-sur-Yvette 91191, France
[i] University of Twente, Enschede 7522 NB, Netherlands
[j] CERN Technology Department, Geneva CH-1211, Switzerland

ARTICLE INFO

Article history:
Received 13 November 2024
Revised 24 April 2025
Accepted 27 May 2025
Available online 3 June 2025

Keywords:
Fusion magnet
High-temperature superconductor
REBCO CICC
Electromagnetic and thermal load
Operational stability

ABSTRACT

A promising way to realize controlled nuclear fusion involves the use of magnetic fields to control and confine the hot plasma configuration. This approach requires superconductor magnets operating above 15 T for the next generation of fusion devices. Due to their high in-field transport current capacity, rare-Earth barium copper oxide (REBCO) coated conductors are promising materials for manufacturing of cable-in-conduit conductors (CICCs) for fusion. However, the high-aspect-ratio geometry makes it difficult to find a multi-tape CICC configuration that fulfills the high engineering current density requirements while retaining enough flexibility for winding large-scale magnets. Moreover, the multilayer structure and inherent brittleness make the REBCO tapes susceptible to degradation during CICC manufacturing and operation. For more than a decade, the development of a reliable REBCO-based CICC that can sustain the huge combined mechanical, thermal, and Lorentz loads without degradation has been ongoing, albeit with limited progress. In this paper, we report on a prototype REBCO CICC that can withstand an applied cyclic Lorentz load of at least 830 $kN \cdot m^{-1}$, corresponding to a transport current of 80 kA at 10.85 T and 4.5 K. To our knowledge, this is the highest load achieved to date. The CICC uses 288 tapes wound into six strengthened sub-cables, making it capable of having a current sharing temperature, T_{cs}, of around 39 and 20 K when operated under 10.85 T with a current of 40 and 80 kA, respectively. Scaled to a 20-T peak field and 46.5-kA transport current, this provides a temperature margin of over 10 K with respect to an operating temperature of 4.5 K. In addition, no perceptible transport current performance degradation was observed after cyclic Lorentz loading, cyclic warm-up/cool-down (WUCD), and quench campaigns. The proposed REBCO CICC is a milestone in the development of high-temperature superconductors for large-scale and high-field magnet applications.

1. Introduction

To realize a balance between energy development, environmental protection, and sustainability, major efforts are being made all over the world to promote the development of green energy. One

* Corresponding authors.
E-mail addresses: chao.zhou@ipp.ac.cn (C. Zhou), qinjg@ipp.ac.cn (J. Qin).

https://doi.org/10.1016/j.eng.2025.05.015

promising approach is the production of stable and clean energy by means of deuterium (D) and tritium (T) fusion reactions, as illustrated in Fig. 1 [1], especially relying on magnetic plasma confinement, as in tokamaks [2]. Such a configuration calls for different kinds of superconducting magnets, including toroidal-field (TF), poloidal-field (PF), and central solenoid (CS) coils to provide the poloidal and toroidal magnetic field components that are required for the confinement of a very hot (many millions of degrees Celsius) plasma at a high pressure (tens of megapascals). The strength of the magnetic field is a critical parameter in preventing the plasma from coming into contact with the first wall and thus in achieving these conditions. Furthermore, the produced fusion power is proportional to the strength of the magnetic field to the fourth power. Therefore, future fusion tokamaks such as the European Demonstration Fusion Power Plant (EU-DEMO), the Chinese Fusion Engineering Test Reactor (CFETR), and the American Affordable, Robust, Compact (ARC) reactor require superconducting magnets operating with peak magnetic fields higher than 15 T, even reaching up to 20 T [3–8]. As a result, one of the key technological issues to be resolved for the application of future fusion energy is the development of large-scale and high-field magnet technology beyond the present state of the art.

To fulfill the requirement of providing a high magnetic field in a large volume, numerous ampere-turns are required in a magnet. Cable-in-conduit conductors (CICCs) have been found to be an attractive option for the design and manufacturing of large-scale superconducting fusion magnets [9]. CICCs offer a number of advantages such as mechanical stability, efficient cooling, and low alternating current (AC) losses. The development of CICCs for large-current-capacity superconducting magnet applications can be traced back to the early 1970s [10]. In the last 50 years of development, significant progress has been achieved in the design, manufacturing, and application of superconducting CICCs, with a wide range of layouts being chosen to design and eventually build magnets for high-field test facilities and fusion devices already in operation (Experimental Advanced Superconducting Tokamak (EAST) [11–13]; Korean Superconducting Tokamak Reactor (K-STAR) [14,15]; Japanese Torus-60 Super Advanced (JT-60SA) [16,17]) or under construction (International Thermonuclear Experimental Reactor (ITER) [18,19]). However, all these magnets rely on low-temperature superconductor (LTS) materials such as Nb–Ti and Nb_3Sn, which limit the peak magnetic fields on the conductors during operation to values below 15 T. High-temperature superconductor (HTS) materials [20] such as rare-Earth barium copper oxide (REBCO) tapes and Bi2212 wires show excellent current-carrying performance under a high magnetic field and are promising candidates for field applications well above 15 T.

In recent years, HTS materials have undergone rapid growth, particularly REBCO tapes, which can now be produced in thousand-meter unit lengths by several companies worldwide. The mass-produced tapes continue to show excellent current-carrying performance under high magnetic fields [21,22]. Moreover, REBCO tapes can operate at relatively high cryogenic temperatures of up to around 80 K, which can provide the benefit of significant temperature margins for the magnets to overcome the effects of high thermal loads during operation. All these advances make REBCO tapes a promising candidate for application in next-step fusion magnets. However, technological challenges have been encountered due to the anisotropy and brittleness of the REBCO tape's structure, which make its transport current properties dependent on field orientation and susceptible to performance degradation under high mechanical and/or electromagnetic loads. To find a practical solution to address these issues, various types of REBCO-tape arrangements and CICC design concepts have been proposed [23–25]. These arrangements and concepts combine REBCO tapes for carrying currents ranging from a few to several tens of kiloamperes. Selected representative sub-cables and CICC specimens that have been manufactured and tested under high-magnetic-field conditions are displayed in Fig. 2 [26–29]. To our knowledge, none of these CICCs have demonstrated stable operation for currents higher than 50 kA under the SUpraLeiter Test ANlage (SULTAN) test condition of 10.85 T, since the high electromagnetic and/or thermal loads always induce irreversible performance degradation of the superconductor properties. For the so-called vacuum–pressure-impregnated, insulated, partially transposed, extruded, and roll-formed (VIPER) conductor, which has an operation current of 45 kA and a magnetic field of 10.85 T, only a marginal degradation of no more than 5% was observed [26]. However, for the other different REBCO-based CICC specimens, the maximum degradation was up to around 60% [30–33]. From that perspective, it can be said that the development of REBCO CICC technology is still encountering difficulties in large-scale magnet application. Therefore, it is a priority to find a suitable CICC design concept and non-destructive manufacturing procedures to resolve the performance degradation issues encountered by numerous HTS CICC test samples operating under high electromagnetic and thermal loads.

To satisfy the requirements of a transport current of approximately 45 kA at a peak magnetic field of around 20 T for the next generation of fusion devices, HTS CICC technologies are being investigated by the Institute of Plasma Physics, Chinese Academy of Sciences (ASIPP), in Hefei, China, relying on commercially available REBCO tapes. A great deal of development—through both numerical simulations and trial and error—has been carried out to address the issue of performance degradation under electromagnetic and thermal cyclic loads. In a tokamak magnet system, the most severe operating conditions in terms of cyclic loads are those for the CS, which is also the magnet for which the highest peak field is required. Recently, we have converged toward a REBCO CICC design. A conductor sample we manufactured using this design was tested in a background field of 10.85 T at the SULTAN test facility in Villigen, Switzerland (where 10.85 T is the highest

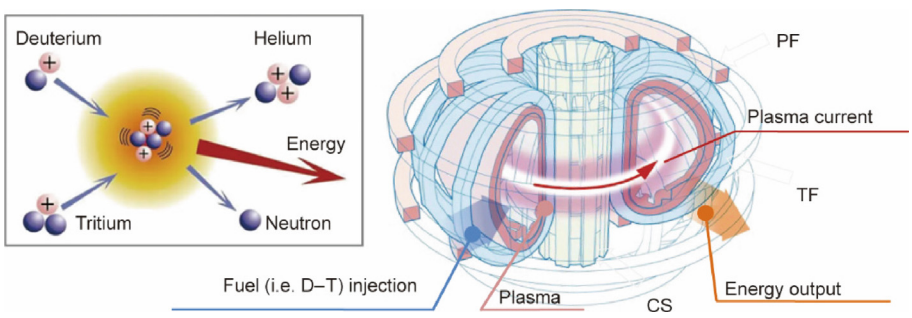

Fig. 1. Schematic drawing of the superconducting magnet system of a tokamak to produce D–T fusion reactions. CS: central solenoid; TF: toroidal-field; PF: poloidal-field. Reproduced from Ref. [1] with permission.

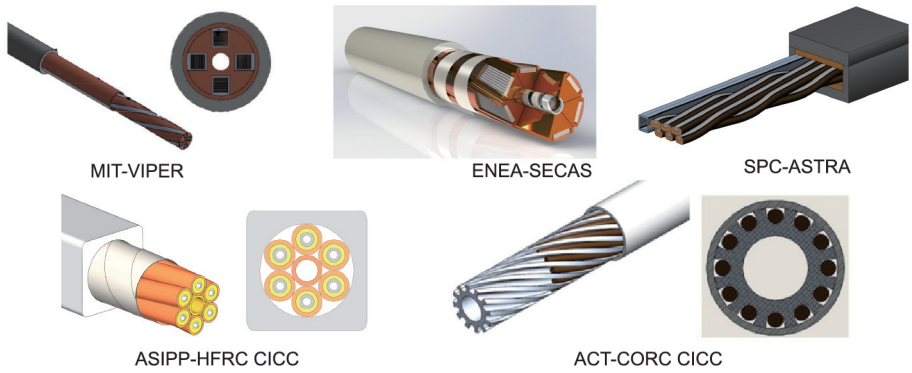

Fig. 2. Examples of different REBCO-based CICCs that have been developed worldwide. Reproduced from Refs. [26–28] with permission. MIT: Massachusetts Institute of Technology; VIPER: vacuum–pressure-impregnated, insulated, partially transposed, extruded, and roll-formed; ENEA: European Nuclear Energy Agency; SECAS: sector assembled cable; SPC: Swiss Plasma Center; ASTRA: aligned stacks transposed in roebel arrangement; ASIPP: Institute of Plasma Physics, Chinese Academy of Sciences; HFRC: highly flexible REBCO cable; ACT: Advanced Conductor Technologies Company; CORC: conductor on round core.

background field presently available for CICC sample testing). The sample reached a stable operation current higher than 80 kA under a 10.85-T background magnetic field. These good results confirm that increasing the mechanical integrity of the individual sub-cables and reinforcing the inter-sub-cable mechanical support in the CICC configuration are critical in overcoming the effects of electromagnetic cyclic loads. Moreover, no performance degradation was observed after repeated warm-up/cool-down (WUCD) and quench campaigns, as well as during and after electromagnetic cycling. These results demonstrate that the proposed design enables a clear step toward a practical REBCO-based CICC for high-field fusion magnet applications that can operate at magnetic fields exceeding 15 T. In the meantime, it may also be a good choice for consideration for any other applications requiring large-scale and high-field magnets, such as hybrid high-field-magnet facilities [34,35] and high-field solenoids for muon colliders [36,37].

2. The REBCO-based CICC design and manufacturing

The applied REBCO-based CICC design proposed herein is displayed in Fig. 3. It is composed of a round cable in a round-in-square stainless-steel (SS) jacket. To increase the mechanical integrity of the sub-cables and of their subsequent arrangement in the final CICC configuration, a number of optimizations and innovations were carried out and implemented. A detailed finite-element model was developed in parallel to describe the mechanical behavior of the CICC [38], assess critical stress concentration points, and propose remedial actions to mitigate them. Major improvements included optimizing the gaps between the wound REBCO tapes from the same layers [39,40], inserting each sub-cable into a 1 mm-thick copper tube, and filling the gaps between the strengthened sub-cables with copper "keystone" segments to prevent deleterious displacements and deformations. The aim of these measures was to homogenize the stress by reducing its peak

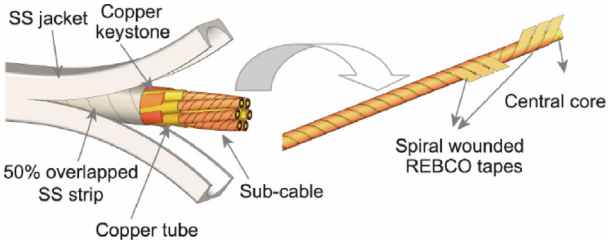

Fig. 3. Schematic drawing of the REBCO-based CICC structure. SS: stainless-steel.

concentrations on the sub-cables and to resist distortion due to the high Lorentz load of up to 900 kN·m^{-1} during CS operation. In this way, the REBCO tapes can be protected from the performance degradation caused by destruction of the REBCO superconducting layers or by exceeding their own irreversible strain limits.

Table 1 summarizes the key design parameters of the proposed REBCO-based CICC. The cable itself is made of six twisted sub-cables wound from 4 mm-wide and 0.1 mm-thick REBCO tapes from Shanghai Superconductor Technology, Inc. (China) [41]. Each sub-cable consists of 48 REBCO tapes helically wound around a 4.6 mm-thick copper core in 16 layers. In addition, there are eight 4 mm-wide and 0.1 mm-thick copper tapes helically wound in two layers on the outer surface of the sub-cable for protection, which is relevant not only for sub-cable transportation but also for subsequent procedures in CICC manufacturing. The gaps between tapes belonging to the same layer were reduced to 0.6 mm; this optimum was chosen to maintain a balance between control over the sub-cable's winding and its bending flexibility. Therefore, the number of wound tapes per layer was increased, starting from the inmost layers and ending with four tapes for the outer layers of the sub-cable. In addition, the jacket was made of a newly developed high-nitrogen material [42] with combined high strength and ductility under cryogenic temperatures. All these measures are expected to ensure good operational stability and, in theory, the ability to withstand a Lorentz load exceeding 1000 kN·m^{-1} [38]. All the operations concerning the insertion of sub-cables into copper tubes, twisting of strengthened sub-cables, and keystone mounting were carried out at the ASIPP conductor workshop, which was set up at the time for ITER conductor manufacturing.

To qualify the transport current stability of the proposed REBCO-based CICC design, CICC samples with a length of 2.77 m (to satisfy the length of HTS CICC sample required by the test equipment at SULTAN) were manufactured with the parameters listed in Table 1, following the main processes displayed in Fig. 4. In total, 288 REBCO tapes were helically wound into six sub-cables. Every sub-cable was inserted into a copper tube, which was then compacted to its final dimensions. The six sub-cables were twisted with a pitch of around 620 mm together with the copper keystones and then secured by the overlapping SS strip. To preserve the mechanical integrity, the entire composite cable was inserted into the jacket and then compacted, decreasing the inner diameter of the jacket to a value equal to the outer diameter of the SS-wrapped CICC cable. Cold rolling was used to compact both the SS jacket and the copper tube around the sub-cable. As shown in Fig. 4, the rollers of the compaction machines were custom-made according to the outer configurations of the jacket and copper tube. The jacket cross-sectional dimensions were

Table 1
Salient parameters of the REBCO-based CICC.

Parameter	Value
Design target	
Critical operation conditions	46.5 kA at 20 T
Inlet temperature	4.5 K
Temperature margin/current sharing temperature	>10 K/> 14.5 K
REBCO tape	
Width × thickness	4 mm × 0.1 mm
Thickness of substrate	50 μm
Total amount of tape per meter CICC	~500 m
Critical current at 77 K and self-field conditions	165–200 A
Critical current at 4.2 K, 12 T	> 410 A
CICC cable	
Number of sub-cables	6
Sub-cable layout (number of wound tapes × layers)	(2 × 4 + 3 × 8 + 4 × 4) REBCO tapes + (4 × 2) copper tapes on outer layers
Number of tapes	48 per sub-cable, 288 in total
Outer diameter of central core for sub-cable	4.6 mm
Gap between wound tapes for sub-cable	(0.6 ± 0.1) mm
Outer diameter of sub-cable	(8.89 ± 0.10) mm
Copper tube around sub-cable and the central tube outer diameter × thickness	(10.9 × 1.0) mm
Outer diameter of twisted cable	(32.8 ± 0.2) mm
SS tape (thickness × width)	(0.1 × 25) mm, 50% overlap
Cable diameter with overlapped SS tape	(33.7 ± 0.15) mm
Void fraction of the whole CICC cable	26%
Twist pitch	(620 ± 20) mm
Jacket	
Material	CHSN01 SS tube
Outer dimensions after conductor forming	42.5 mm × 42.5 mm

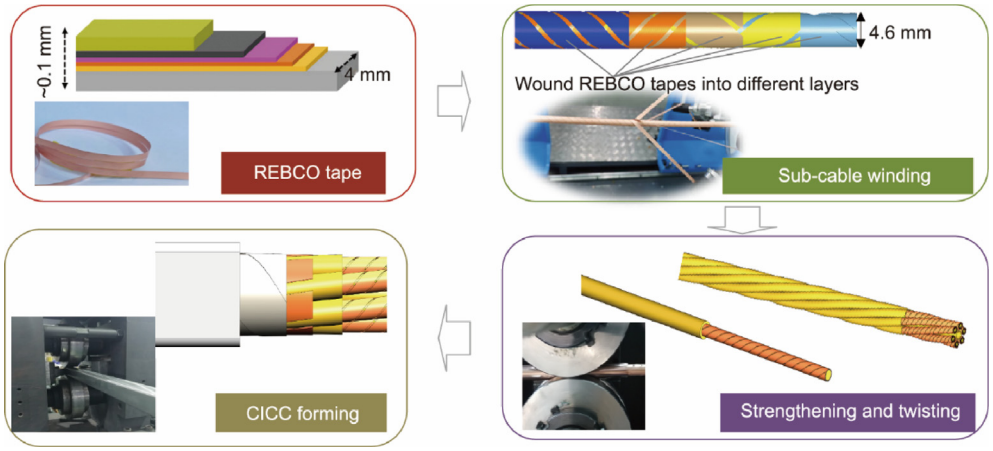

Fig. 4. Scheme of the main processes involved in manufacturing the REBCO-based CICC.

reduced from 43.5 mm × 43.5 mm to 42.5 mm × 42.5 mm, and the inner diameter was decreased from 35 to ~33.8 mm. The outer diameter of the copper tube containing the sub-cable was compacted from 12.5 to 10.9 mm, increasing its thickness from 0.90 to ~0.95 mm. Fig. 5 shows the configuration of the wound REBCO cable before and after being braced with the copper tube, as well as the manufactured REBCO-based CICC with its termination, which has a length of 330 mm, a width of 64 mm, and a height of 41 mm. The termination box was made of SS and oxygen-free copper, which were connected by brazing. The cable with staged tapes was inserted into the termination box and filled with PbSn solder. Finally, the SS parts were interlinked by means of manual welding.

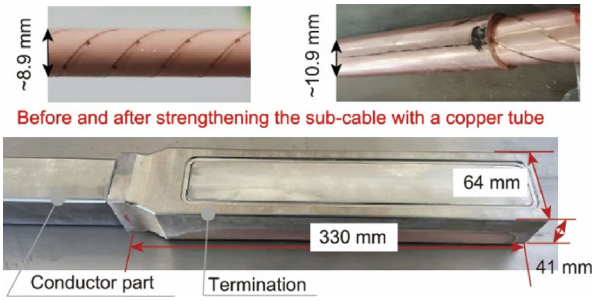

Fig. 5. Pictures of the main components of the manufactured REBCO-based CICC specimen.

3. Performance testing at cryogenic temperatures and under a high magnetic field

3.1. Testing of specimen preparation

The aforementioned REBCO-based CICC specimen was assembled in view of its mounting at the SULTAN test facility. Two 2.77 m-long conductor sections were manufactured according to the design shown in Fig. 3. The only difference between the two CICC sections was the central core used for sub-cable winding: one contained a stainless spiral tube and the other relied on an

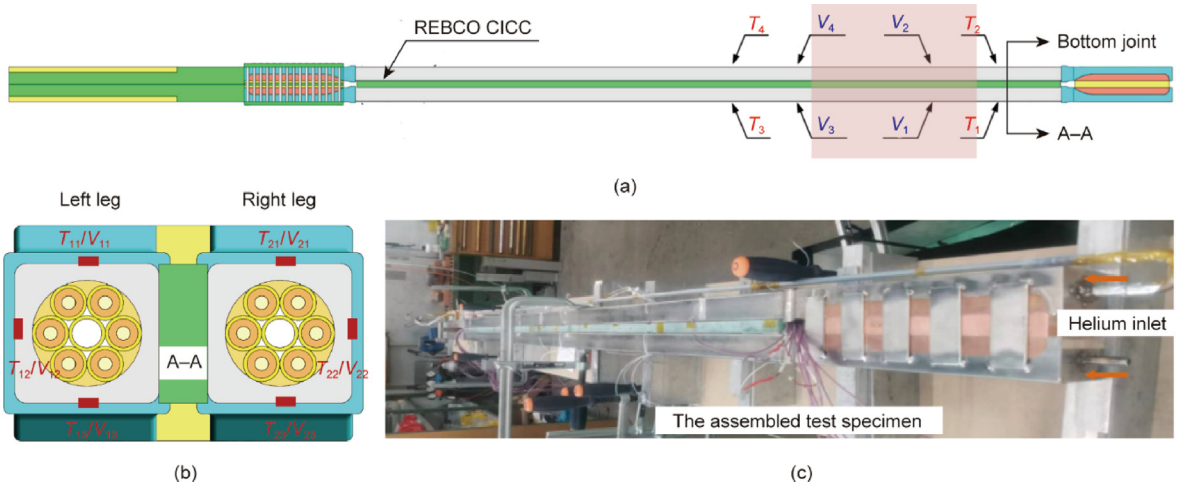

Fig. 6. Schematic of the instrumentation and view of the assembled ASIPP REBCO-based CICC test specimen at SULTAN. (a) Schematic of a CCIC legs; (b) distribution of voltage taps *V* and temperature sensors *T*; (c) the assembled test specimen.

oxygen-free copper rod. The two CICC sections were assembled together by means of SS and glass epoxy clamps to form a hairpin-shaped sample. The leg whose sub-cables were wound with oxygen-free copper rods was assembled as the right (R) leg. The other leg, which had sub-cables wound with a stainless spiral tube, was assembled as the left (L) leg. Both legs were electrically connected by a bottom joint and were tested simultaneously at cryogenic temperatures against a background magnetic field of up to 10.85 T. Crown arrays of temperature sensors and voltage taps were assembled at several axial locations along the jacket of the two CICC legs to detect the superconducting-to-normal transition of the CICC specimens during operation. The main focus was around the high-field area, shaded in pink in Fig. 6(a), which had a length of around 450 mm. The two sets of temperature sensors and voltage taps assembled near the borders of the high-field zone were used to assess the critical current-carrying performance. For every instrumented cross-section of the CICC, there were three voltage taps (labeled *V* in Fig. 6) and three temperature sensors (labeled *T*) mounted on adjacent sides of the conductor jacket; their distribution is shown by the rectangular red shapes in Fig. 6(b). The assembled test specimen is shown in Fig. 6(c). The helium coolant flows in from the bottom termination and flows out at the upper terminals of both CICC legs. The focus of this manuscript is on the specimen assembled on the right leg (with copper rods in the sub-cables), which exhibited a more stable performance under the high-magnetic-field operation conditions.

3.2. Performance evaluation under a 77-K self-field

A test was carried out in liquid nitrogen at ASIPP prior to the assemblage at the SULTAN test facility. The aim of the test was to assess the reliability of the applied manufacturing processes in avoiding any damage to the fragile REBCO tapes. For the test, the CICC samples were immersed into liquid nitrogen and connected to a 100-kA direct current (DC) power supply. Fig. 7 shows the expected self-field distribution on the cable for an operation current of 6 kA, which is supposed to be evenly distributed among the sub-cables. The peak field is about 0.06 T, which yields a factor of approximately 0.01 T·kA^{-1} for self-field correction during operation. Fig. 8 shows the measured electrical field as a function of the transport current, with the electrical field being measured from the assembled voltage taps; V_3–V_1 and V_4–V_2 show the same variation trends with the current injection. The plot displays a slight initial slope (~2 × 10^{-4} μΩ·cm^{-1}) before the superconducting-to-normal transition occurs. This initial voltage is likely caused by ① the current through the copper parts of the CICC cross-section, ② the contact resistances among the wound tapes, and ③ the uneven distribution of the current among the wound REBCO tapes, which was mainly introduced at the terminations. The measured critical current at 77 K and the maximum self-field of 0.23 T is around 22.6 kA when using a criterion of 1 μV·cm^{-1} after removing

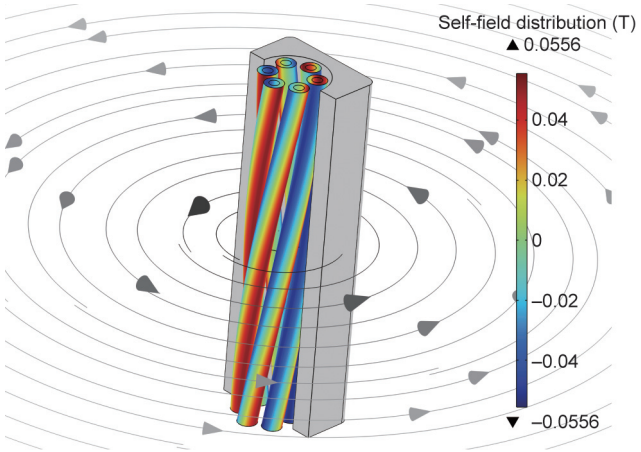

Fig. 7. The computed self-field generated on the cable when carrying a current of 6 kA (1 kA per sub-cable).

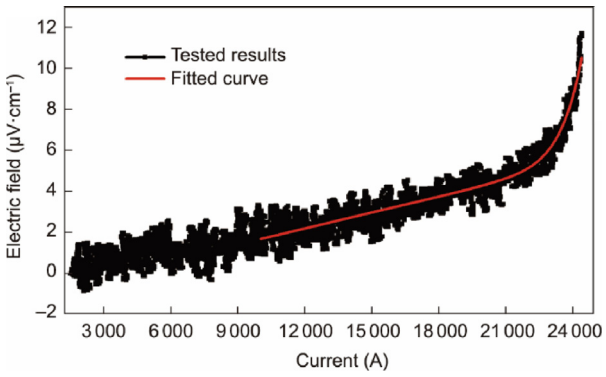

Fig. 8. Electric field of the REBCO-based CICC as a function of current at 77 K under a self-field.

the offset from the slope. This result is in good agreement with the value of approximately 21 kA that was estimated using the average tape performance from the supplier. In addition, an n value of about 22 can be derived from the data in the 0.1–1 $\mu V \cdot cm^{-1}$ range in Fig. 8, which is equivalent to that of a single tape. These results confirm that the manufacturing process does not seem to have resulted in any measurable tape degradation.

3.3. Overall stability under a high magnetic field

To assess the mechanical stability, sensitivity to temperature variation, and robustness to quenching of the REBCO CICC, the manufactured sample was tested at the SULTAN facility. Tests including electromagnetic force, WUCD and quench cycling were carried out on the CICC specimens. The WUCD and quench tests were performed in combination with electromagnetic cycling runs. To assess whether any degradation had occurred during the various phases of the test campaign, the current sharing temperature (T_{cs}) at 40 kA and under a 10.85-T background magnetic field was selected as a benchmark. Before and after all tests, the T_{cs} at 40 kA and 10.85 T was measured by slowly raising the temperature of the cooling medium (liquid helium). The T_{cs} under those conditions was estimated based on the following fitting equation with a criterion of 1 $\mu V \cdot cm^{-1}$:

$$EF = (T/T_{cs})^m + R_0 T + EF_0 \quad (1)$$

where EF_0 represents the resistive offset electrical field, m is a fitting parameter, and R_0 represents the calculated slope in the tested electrical field versus temperature plots. Details for each test and the results are described in the following sections.

3.3.1. Electromagnetic cycling performance

The electromagnetic force acting on the CICC was generated by supplying a DC into the CICC sample at 4.5 K under a background magnetic field of 10.85 T. To avoid missing the critical point of possible performance degradation at low electromagnetic force, the current was increased in a stepwise manner from 40 to 80 kA. The DC loads used for the electromagnetic cycling are shown as magenta dots in Fig. 9. The figure shows the evolution of the T_{cs} assessed at 40 kA and 10.85 T at regular intervals over a total of 1267 electromagnetic cycles carried out at increasingly higher current levels. There are three calculated T_{cs} plots corresponding to estimates based on the three different temperature sensors mounted on the conductor jacket of the R-leg (shown in Fig. 6(b)). The plots show no sign of T_{cs} degradation, even after current cycles up to 80 kA at 10.85 T and 4.5 K. A fluctuation of less than 1 K was observed at around 700 load cycles, after the cycling current had been raised to 55 kA. The likely cause for this fluctuation is that it was decided to reverse the current direction in the two legs at that time. This change in current polarity changed the direction of the Lorentz load and the position of the stress concentration point from one side of the CICC to the other, as illustrated at the bottom of Fig. 9. The change of the cable-to-jacket contact side may in turn have caused a different temperature distribution in the two-dimensional cross-section of the CICC. This explains the observed fluctuation measured by temperature sensor T_{22}, which—given its position at the CICC mid-plane—was the most affected.

The achieved stable operation current of 80 kA under a background magnetic field of 10.85 T (the field on the sample is around 10.4 T, due to the reversed self-field) and at 4.5 K corresponds to an electromagnetic load of approximately 830 $kN \cdot m^{-1}$. Achieving an even higher current is still possible for this sample, since the test was stopped due to a high resistance in the test circuit localized at the bottom joint, which might have been caused by a non-conformity in the joint manufacture. This was also the reason for the reversal of current direction applied at 55 kA. Therefore, we plan to re-assemble the successful leg of this sample using another REBCO-based CICC specimen to check its operational limits in the near future. This 80-kA current represents 94% of the expected peak load in the CS of the next-generation fusion device in China, which is designed to operate with a maximum current of 46.5 kA and a peak field of about 20 T.

3.3.2. Thermal cycling

Long-term operation of fusion machines (and other devices) will impose multiple WUCD cycles on the magnet between 4.5 K and room temperature during its lifetime. Therefore, we also paid attention to the effects of the WUCD cycles on the CICC's current carrying capacity and stability. The first WUCD cycle was carried out after 600 electromagnetic cycles, with a current cycling between zero and 47 kA; a second WUCD cycle was carried out after completing the electromagnetic cycling tests. Fig. 10 shows the measured T_{cs} at 40 kA and 10.85 T before and after the WUCD cycles, where the T_{cs} evaluation used the measured maximum temperature from the jacket surfaces, as shown in Figs. 6 and 9. The first WUCD cycle was carried out before reversing the current direction, and the T_{cs} values before and after the WUCD are almost

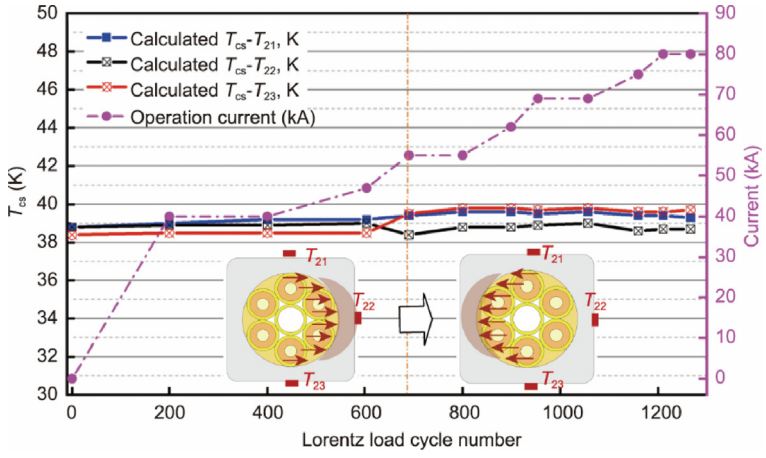

Fig. 9. Evolution of T_{cs}, measured at regular intervals over a sequence of electromagnetic cycling at increasing Lorentz load values from 450 to 830 $kN \cdot m^{-1}$, carried out at 10.85 T and 4.5 K. The three T_{cs} curves correspond to assessments carried out for the three different temperature sensors mounted on the CICC jacket. A minor fluctuation of less than 1 K for the estimated current sharing temperatures was observed around 700 cycles, likely due to a change in the transport current polarity, which was applied starting at an operating current of 55 kA.

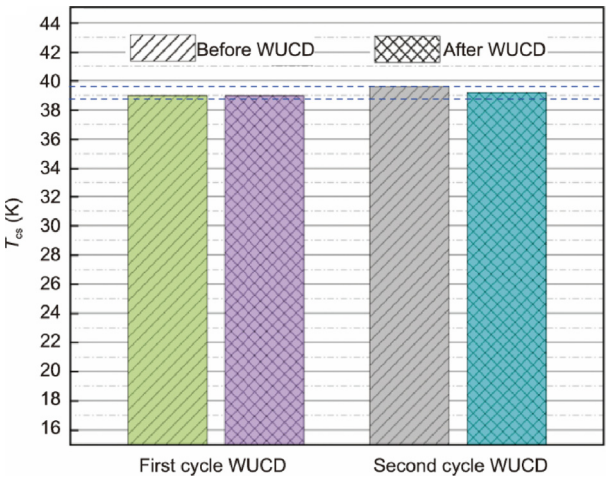

Fig. 10. T_{cs} at 40 kA and 10.85 T, measured before and after the first and second WUCD cycles.

equal. However, the second WUCD cycle was carried out at the end of the electromagnetic cycling at 80 kA, after the current direction reversal, and the T_{cs} values are based on temperature sensors mounted on different sides (i.e., the T_{23} sensor shown in Fig. 10) of the CICC jacket. The value before the second WUCD cycle is around 0.6 K higher than the value after the first WUCD. The value after the second WUCD is around 0.4 K lower than that before the second WUCD, but it is still 0.2 K higher than the value after the first WUCD cycle. The fact that the values before and after the second WUCD are higher than the values before and after the first WUCD can be explained by the fact that the cable peak field on the cable dropped by about 0.45 T as a result of the current direction reversal that was applied in between. The slight decrease in T_{cs} before and after the WUCD may be within the error bar of this difficult measurement; at this stage, therefore, it can be concluded that the WUCD cycles do not seem to have a strong impact on the CICC performance.

3.3.3. Quench performance

The T_{cs} measurements were carried out by fixing the current and magnetic field and then increasing the temperature of the cooling medium until the superconducting-to-normal transition occurred. Thus, every T_{cs} measurement at 40 kA and 10.85 T was stopped by quenching the samples, and these quenches did not appear to result in any noticeable performance degradation. To confirm this result, it was decided to provoke additional quenches at different current levels and assess whether higher electromagnetic loads would have an impact. Additional quench campaigns were then carried out. The test processes were similar to those used for T_{cs} testing. The background magnetic field was fixed at 10.85 T, while the current was changed from 47 to 55 kA and then to 65 kA in a stepwise manner. The test was stopped by switching off the power supply when the voltage caused by the quenching exceeded a certain threshold, as set by the lab to protect both the whole test system and the sample. Fig. 11 illustrates the electric field versus the rising temperature measured on the CICC jacket by letting the current and magnetic field remain fixed until a quench occurred.

Based on the nonlinear fitting described above, the results were T_{cs} of about 34.5 K at 47 kA, about 30 K at 65 kA, and about 25.5 K at 65 kA. A total of three quenches were initiated at a current of 80 kA at the end of all DC tests. After the completion of all mentioned quench cycles, a last reference test was carried out at 40 kA under a 10.85-T background magnetic field, which provided a T_{cs} of 39.3 K with a criterion of 1 μV·cm^{-1}. This result means that no noticeable performance degradation occurred during the quench cycles—at least, under the condition of having an active quench protection system for electric fields exceeding 20 μV·cm^{-1}. It is important to note that the initial low slopes of less than 0.5 uV·(cm·K)$^{-1}$ seen on the curves in Fig. 11 are likely due to current non-uniformity resulting from the short length of the bottom joint (i.e., about half of the CICC twist pitch) in combination with the relatively high contact resistance among the wound tapes [24]. In order to confirm the feasibility of and the parameters to be used for a protection system of a REBCO-based CICC in a fusion magnet system, a longer CICC unit length will be tested in the near future as an insert coil.

3.4. Calculated operation performance for fusion magnet application

Fig. 12 presents a summary of predicted versus measured T_{cs} for the REBCO-based CICC while carrying different currents at 10.85 T. Because the predicted T_{cs} uses the average critical current data from the REBCO tape supplier and does not take into account the effects from stress, strain, and current non-uniformity, the measured values are slightly below the predictions. However, the fact that the difference between the two curves is nearly constant and around 2 K indicates that we are not far off and that we can still produce a reliable T_{cs} prediction for the operating conditions of future fusion magnet applications. For the proposed and manufactured CICC, the predicted T_{cs} versus the operation current at 20 T is shown as a purple dotted line in Fig. 12. For 46.5 kA at 20 T, we can expect the temperature margin to be higher than 15 K with respect to an operating temperature of 4.5 K.

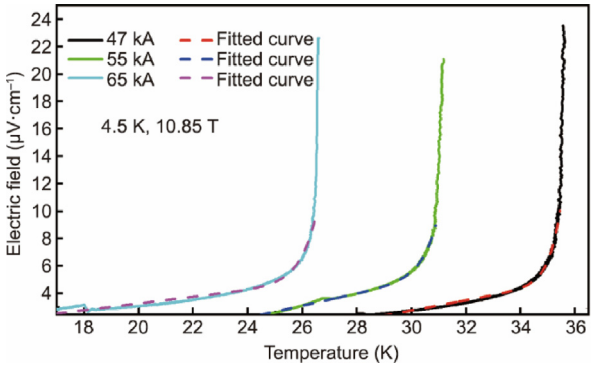

Fig. 11. *E*–*T* plots of the REBCO-based CICC sample at different currents under a background magnetic field (*B*) of 10.85 T.

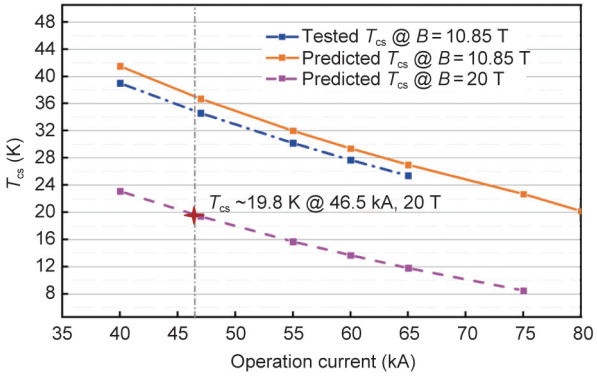

Fig. 12. Predicted and tested T_{cs} at 4.5 K under different magnetic field conditions.

4. Conclusions

In this work, we presented the details of the design, manufacturing, and test results of one type of HTS CICC made of REBCO tapes. The design was proposed for applications requiring a high transport current and a magnetic field beyond 15 T, as is the case for superconducting magnets for next-generation fusion devices. Based on the results presented above, the main conclusion to be drawn is that the newly designed and tested REBCO-based CICC specimen can operate reliably under critical conditions such as high electromagnetic and thermal cyclic loads and sudden quench events.

The results show that REBCO tapes have potential to meet the most rigorous stability requirements needed for the next generation of fusion devices (i.e., operation with a maximum current of 46.5 kA at a peak field of around 20 T and a nominal temperature of 4.5 K). As long as the tapes are implemented in an appropriate CICC architecture and the manufacturing procedures are well controlled, the operation parameters can even be higher. However, there are still some key issues to be overcome before the suitability of REBCO tapes can be fully demonstrated for fusion magnet applications, including but not limited to ① scaling of the manufacturing technology to allow long CICCs; ② AC loss evaluation and control during demanding plasma scenarios; ③ high-precision coil winding; ④ reliable, low-resistance splices; and ⑤ sensitive quench detection and robust quench protection for large-scale magnets. Following this important first step and achievement, our focus will now shift to addressing all these issues in a systematic and rigorous manner. Despite these challenges, we have a high degree of confidence that, in the near future, large-scale and high-field REBCO magnet technology can be used in the construction of the next generation of fusion devices.

CRediT authorship contribution statement

Huan Jin: Writing – original draft, Investigation, Formal analysis, Data curation. **Guanyu Xiao:** Resources, Investigation. **Chao Zhou:** Writing – review & editing, Formal analysis, Conceptualization. **Chuanyi Zhao:** Resources. **Shijie Shi:** Resources. **Haihong Liu:** Resources. **Fang Liu:** Validation, Resources, Data curation. **Huajun Liu:** Validation, Resources, Data curation. **Yu Wu:** Validation, Resources, Data curation. **Zuojiafeng Wu:** Resources. **Hugues Bajas:** Validation, Resources, Data curation. **Jack Greenwood:** Validation, Resources, Data curation. **Mattia Ortino:** Validation, Resources, Data curation. **Kamil Sedlak:** Validation, Resources, Data curation. **Valentina Corato:** Writing – review & editing. **Richard Kamendje:** Project administration, Funding acquisition. **Alexandre Torre:** Writing – review & editing. **Arend Nijhuis:** Writing – review & editing, Validation. **Giulio Anniballi:** Validation, Investigation. **Arnaud Devred:** Writing – review & editing, Validation, Formal analysis. **Jinggang Qin:** Supervision, Project administration, Investigation. **Yuntao Song:** Funding acquisition. **Jiangang Li:** Funding acquisition.

Declaration of competing interest

The authors declare that they have no known competing financial interests or personal relationships that could have appeared to influence the work reported in this paper.

Acknowledgments

This work was partly supported by the Comprehensive Research Facility for the Fusion Technology Program of China (2018-000052-73-01-001228), the National Key Research and Development Program of China (2022YFE03150200), the Institute of Energy, Hefei Comprehensive National Science Center (21KZS207), the National Natural Science Foundation of China (52077212), the Youth Innovation Promotion Association of the Chinese Academy of Sciences (2021444), and the European–China collaboration program on the FUSION magnet.

References

[1] Conservation laws in nuclear reactions [Internet]. Nuclear Power; [cited 2024 Nov 13]. Available from: https://www.nuclear-power.com/laws-of-conservation/conservation-laws-in-nuclear-reactions/.
[2] Degrave J, Felici F, Buchli J, Neunert M, Tracey B, Carpanese F. Magnetic control of tokamak plasmas through deep reinforcement learning. Nature 2022;602:414–9.
[3] Leslie M, Ito T, Aizawa K, Arima H. Start-ups seek to accelerate path to nuclear fusion. Engineering 2021;8:6–8.
[4] Corato V, Vorpahl C, Sedlak K, Anvar VA, Bennet J, Biancolini ME, et al. The DEMO magnet system—status and future challenges. Fusion Eng Des 2022;174:112971.
[5] Sedlak K, Anvar VA, Bagrets N, Biancolini ME, Bonifetto R, Bonne F, et al. Advance in the conceptual design of the European DEMO magnet system. Supercond Sci Technol 2020;33(4):044013.
[6] Zheng J, Song Y, Liu X, Li J, Wan Y, Ye M, et al. Concept design of hybrid superconducting magnet for CFETR tokamak reactor. In: Proceedings of 2013 IEEE 25th Symposium on Fusion Engineering (SOFE); 2013 Jun 10–13; San Francisco, CA, USA. IEEE; 2013.
[7] Greenwald M, Whyte D, Bonoli P, Hartwig Z, Irby J, LaBombard B, et al. The high-field path to practical fusion energy. Report. Cambridge: Massachusetts Institute of Technology; 2018.
[8] Sorbom BN, Ball J, Palmer TR, Mangiarotti FJ, Sierchio JM, Bonoli P, et al. ARC: a compact, high-field, fusion nuclear science facility and demonstration power plant with demountable magnets. Fusion Eng Des 2015;100:378–405.
[9] Hoenig M, Montgomery D. Dense supercritical-helium cooled superconductors for large high field stabilized magnets. IEEE Trans Magn 1975;11(2):569–72.
[10] Dresner L. Twenty years of cable-in-conduit conductors: 1975–1995. J Fusion Energy 1995;14:3–12.
[11] Wan YX. Overview of steady state operation of HT-7 and present status of the HT-7U project. Nucl Fusion 2000;40:1057–68.
[12] Wu Y. Experience in operating safety of EAST superconducting magnets. IEEE Trans Appl Supercond 2010;20(3):431–7.
[13] Li J, Wan Y. The experimental advanced superconducting tokamak. Engineering 2021;7(11):1523–8.
[14] Hahn SH, Kim KH, Choi JH, Ahn HS, Lee DK, Park KR, et al. Controls on KSTAR superconducting poloidal field (PF) magnets. Prog Supercond Cryog 2008;10(4):23–8.
[15] Lim BS, Lee SI, Choi JY, Chung W, Chu Y, Park HK, et al. Development of CICC for KSTAR TF coil system. IEEE Trans Appl Supercond 2003;13(2):1496–9.
[16] Ishida S, Barabaschi P, Kamada Y. Status and prospect of the JT-60SA project. Fusion Eng Des 2010;85(10–12):2070–9.
[17] Sharma RG. Superconducting magnets in fusion reactors. In: Superconductivity: basics and applications to magnets. Cham: Springer; 2021.
[18] Mitchell N, Bessette D, Gallix R, Jong C. The ITER magnet system. IEEE Trans Appl Supercond 2008;18(2):435–40.
[19] Devred A, Backbier I, Bessette D, Bevillard G, Gardner M, Jong C, et al. Challenges and status of ITER conductor production. Supercond Sci Technol 2014;27:044001.
[20] Molodyk A, Larbalestier DC. The prospects of high-temperature superconductors. Science 2023;380(6651):1220–2.
[21] Tsuchiya K, Wang X, Fujita S, Ichinose A, Yamada K, Terashima A, et al. Superconducting properties of commercial REBCO-coated conductors with artificial pinning centers. Supercond Sci Technol 2021;34(10):105005.
[22] Paidpilli M, Goel C, Sarangi B, Chen S, Galstyan E, Jaroszynski J, et al. 40-meter-long REBCO tapes with critical current over 4000 A/12 mm at 4.2 K and 13 T by advanced MOCVD. Superconductivity 2024;9:100081.
[23] Wang J, Kang R, Chen X, Yang C, Wang Y, Wang C, et al. Development of a Roebel structure transposed cable with in-plane bending of REBCO tapes. Superconductivity 2022;3:100019.
[24] Yagotintsev K, Anvar VA, Gao P, Dhalle MJ, Haugan TJ, Van Der Laan DC, et al. AC loss and contact resistance in REBCO CORC®, Roebel, and stacked tape cables. Supercond Sci Technol 2020;33(8):085009.
[25] Li X, Tang Y, Xu Y, Ren L. Analytical analysis of hollow CORC cable under thermo-mechanical loads. Superconductivity 2023;5:100037.
[26] Hartwig ZS, Rui F, Vieira BN, Sorbom RA, Badcock MB, Beck WK, et al. VIPER: an industrially scalable high-current high-temperature superconductor cable. Supercond Sci Technol 2020;33(11):11LT01.
[27] Corato V, Bruzzone P, Bykovskiy N, Celentano G, Della Corte A, Demattè F. Strategy for developing the EU-DEMO magnet system in the concept design phase. IEEE Trans Appl Supercond 2022;32(6):4201407.
[28] Muzzi L, Augieri A, Celentano G, Chiarelli S, della Corte A, De Marzi G. Design and feasibility assessment of an HTS sector shaped high-current conductor for fusion coils. IEEE Trans Appl Supercond 2023;33(5):4200106.
[29] Weiss J, Van der Laan D, Radcliff K, Doenges S, Jager A, Johnson Z, et al. Development and testing of high temperature superconducting CORC®

magnets and CICC for fusion applications. In: Proceedings of the Applied Superconductivity Conference; 2024 Sep 1–6; Salt Lake City, UT, USA.
[30] Mulder T, Fleiter J, Willering G, Dudarev A, Mentink M, Dhallé M, et al. Demonstration of the ReBCO CORC 47kA@10T/4.2 K cable-in-conduit-conductor and its joint terminals at 4.5 and 77 K. IEEE Trans Appl Supercond 2017;27(4):1–4.
[31] Uglietti D, Bykovsky N, Sedlak K, Stepanov B, Wesche R, Bruzzone P. Test of 60 kA coated conductor cable prototypes for fusion magnets. Supercond Sci Technol 2015;28(12):124005.
[32] Corato V. Overview on present and future deliverables. In: Proceedings of European–China Meeting; 2023 Nov 21; Hefei, China.
[33] Mulder T, Weiss J, van der Laan D, Dudarev A, Kate H. Recent progress in the development of CORC cable-in-conduit conductors. IEEE Trans Appl Supercond 2020;30(4):1–5.
[34] Gupta R, Anerella M, Ghosh A, Lalitha SL, Sampson W, Schmalzle J, et al. Hybrid high-field cosine-theta accelerator magnet R&D with second-generation HTS. IEEE Trans Appl Supercond 2015;25(3):1–4.
[35] Wang Q, Liu J, Zheng J, Qin J, Ma Y, Xu Q, et al. Progress of ultra-high-field superconducting magnets in China. Supercond Sci Technol 2021;35 (2):023001.
[36] Gupta R, Anerella M, Ghosh A, Joshi P, Kirk H, Lalitha SL, et al. High field HTS solenoid for a muon collider—demonstrations, challenges, and strategies. IEEE Trans Appl Supercond 2013;24(3):1–5.
[37] Fabbri S, Bottura L, Quettier L, Statera M, Boattini F, Mariotto S, et al. Magnets for a muon collider. J Phys Conf Ser 2024;2687(8):082016.
[38] Nijhuis A, Anniballi G, van Dusschoten N, Rietber J, Anvar VA, Jin H, et al. Performance prediction and optimization of ReBCO CICC. In: Proceedings of European–China Meeting; 2023 Nov 21; Hefei, China.
[39] Van Der Laan D, McRae DM, Weiss JD. Effect of transverse compressive monotonic and cyclic loading on the performance of superconducting CORC® cables and wires. Supercond Sci Technol 2018;32(1):015002.
[40] Lai XQ, Zuo JX, Hu XB, Zhang T, Liu JD, Li PY. Experimental investigation of axial tensile and fatigue behaviors of HTS round strands. Superconductivity 2023;8:100069.
[41] Shsctec.com [Internet]. Shanghai: Shanghai Superconductor Technology, Inc.; c2025 [cited 2025 May 27]. Available from: https://www.shsctec.com/products/tape.
[42] Wang W, Zhao C, Jin J, Shi J, Tu Z, Chen X, et al. The research on high-strength CICC jackets with YS > 1500 MPa at 4.2 K for future fusion applications. Nucl Mater Energy 2023;36:101474.